ANNALS OF GEOPHYSICS, 65, 4, VO428, 2022; doi:10.4401/
ag-8787 OPEN ACCESS

Near real-time filtering of high precision borehole strainmeter signals for volcano surveillance

Luigi Carleo[*,1], Alessandro Bonaccorso[1], Gilda Currenti[1] and Antonino Sicali[1]

(1) Istituto Nazionale di Geofisica e Vulcanologia, Sezione di Catania – Osservatorio Etneo, Catania, Italy

Article history: received December 30, 2021; accepted April 13, 2022

Abstract

Volumetric strain signal recorded by the Sacks-Evertson strainmeter has a very high resolution and can measure small strain changes (down to 10^{-9}) accompanying volcanic processes. However, different disturbing components perturb the recorded strain signal. These disturbances can mask ultra-small strain changes related to volcano activity and thus need to be filtered in order to accurately monitor volcano deformation. We developed the software STRALERT (STRain and wArning signaLs in nEar Real-Time) to provide both the recorded and the filtered strain signals in near real-time to the Surveillance Room of the "Istituto Nazionale di Geofisica e Vulcanologia – Osservatorio Etneo" which monitors the Etna activity. The software encloses a modified version of the code BAYTAP-G for filtering the incoming signal from the continuously running strainmeter at Etna. Thanks to the appropriate and robust signal filtering, STRALERT is capable to provide an efficient estimate of transient strain changes, which concur in tracing volcano deformation and detecting the onset and the conclusion of eruptive events. Our findings demonstrate the important contribution of STRALERT for volcano surveillance operations.

Keywords: Etna volcano; Strain; Borehole dilatometer; Volcano monitoring; Eruptive activity detection

1. Introduction

Volcanic activity usually produces deformation of the shallow crust that precedes and accompanies paroxysmal phases of eruptive events [i.e. Dzurisin, 2007]. The monitoring and the interpretation of deformation processes are thus crucial for both characterizing the deformation sources and conducting volcano surveillance operations. To these scopes, the Sacks-Everton borehole strainmeters [Sacks et al., 1971] are key instruments since they can record volumetric strain changes of the surrounding rocks with a very high resolution [i.e. Roeloffs and Linde, 2007]. Several installations of borehole strainmeters have been performed in volcanic areas worldwide: Mauna Loa, Hawaii [Linde and Sacks, 1995], Hekla, Iceland [Linde et al., 1993], Soufriere Hills, Montserrat [Voight et al., 2006], Campi Flegrei, Italy [Amoruso et al., 2015], Stromboli, Italy [Bonaccorso et al., 2012], Izu-Oshima, Japan [Linde et al., 2016], Etna, Italy [Bonaccorso et al., 2016].

The strain signal recorded by the borehole strainmeters is usually affected by different disturbing components, mainly due to tidal forces, local barometric pressure, precipitations and underground water circulations [i.e.

Furuya and Fukodome, 1986; Agnew, 1986]. In particular, the tidal and the atmospheric pressure components are the main disturbing signals since they are persistent over time and exhibit amplitudes of the order of 10^{-8} to 10^{-7} masking the strain changes due to volcanic processes. Currenti and Bonaccorso [2019] clearly showed that filtering out both the tidal and pressure components allows to enlighten ultra-small strain changes of the order of 10^{-9} due to pressurization/depressurization cycles of magmatic chamber which regulates the occurrence of summit eruptive events. Detecting these changes accurately is fundamental for monitoring the evolution of the volcano state and have information about the timing of the onset of eruptive events [Bonaccorso et al., 2016]. Therefore, the availability of filtered strain signal has an obvious advantage for monitoring the volcano dynamic. In literature, different softwares have been developed for the strain signal filtering [Tamura et al., 1991; Wenzel, 1996; Amoruso et al., 2000; Venedikov et al., 2003; Langbein, 2010]. These codes were not designed to be run automatically but to be used under the control of an operator who can choose the most suitable model for the recorded strain signal and appropriately manage measurement problems such as gaps, outliers and steps. In near real-time, the automatic use of these software to filter data, which are affected by measurement problems or by strain contributions neglected in the model, could lead to an inaccurate estimation of the filter parameters. This could cause incorrect data processing and misinterpretation of the ongoing deformation with important consequences for volcano surveillance operations. For these reasons, it is advisable to estimate the filter parameters in advance in optimum conditions and, then employ them for near real-time applications, as done for corrections of gravimetric measurements [Van Camp et al., 2017].

To automate the filtering of the strain signal, we developed a new software called STRALERT. It automatically reads the strain signal recorded by the borehole strainmeter network installed on the Etna volcano, performs the strain signal filtering, and transfers it to the Surveillance Room of the "Istituto Nazionale di Geofisica e Vulcanologia – Osservatorio Etneo (INGV-OE)". The program encloses an updated version of the BAYTAP-G code, that has been optimized for near real-time filtering, which allows using a fixed set of pre-estimated filter parameters as inputs.

The problems related to signal filtering in near real-time are widely described in Sect. 2. The procedure employed for the estimation of the filter parameter and the evaluation of the filtering performances are illustrated in Sect. 3 and Sect. 4, respectively. The proposed software approach is presented in Sect. 5. Conclusions are discussed in Sect. 6.

2. Strain signal filtering in near real-time at Etna volcano

At Etna volcano, four borehole strainmeters were installed over the last decade (Figure 1). Each instrument exhibited a different final response depending on the type of rock in which it was installed and on the rock-sensor coupling. The strainmeter placed at Monte Ruvolo (DRUV) is characterized by a very high accuracy. It is capable of clearly recording large strain changes ($\approx 10^{-7}$) due to volcanic events, such as strong lava fountains [Bonaccorso et al., 2016; Bonaccorso et al., 2021], but also small strain changes associated to Earth tides ($\sim 10^{-8}$) and strong teleseism events (at DRUV in the range 10^{-9}-10^{-8}), respectively [Bonaccorso et al., 2016; Currenti et al., 2017].

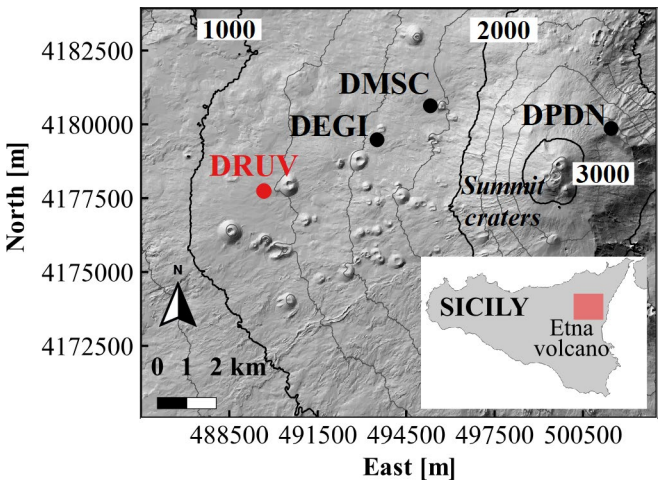

Figure 1. Map of the Etna volcano with the strainmeter network. The coordinates system is WGS 84 UTM 33.

Moreover, the DRUV signal was optimally calibrated using three different methods by comparing the records with theoretical tides [Bonaccorso et al., 2013], synthetic straingrams due to strong teleseisms [Bonaccorso et al., 2016] and strain estimated by a broad-band seismic array for a teleseismic event [Currenti et al., 2017].

The three methods provided comparable calibration factors. These important findings showed that the recorded DRUV signal can provide robust and reliable estimates of the ongoing volcano deformation and thus it was selected to be employed for the near real-time monitoring operations carried out by the INGV-OE Surveillance Room. However, the presence of disturbing components in the strain signals, most relevant of which are due to Earth tides, atmospheric pressure variations, precipitations and underground water circulations, could mask deformation processes related to the volcano activity which knowledge is fundamental for the surveillance operations. Indeed, Currenti and Bonaccorso [2019] showed that an appropriate filtering of the DRUV signal can clearly reveal ultra-small strain changes ($\approx 10^{-9}$) that can be related to inflation/deflation cycles of the volcano edifice concurrently with periods of accumulation/withdrawal of magma in storage zones. In order to provide this clear information for surveillance operations, it is necessary to provide in near real-time the filtered strain signal which should be as robust as possible. To date, different softwares can be employed to perform the signal filtering. The most used codes are BAYTAP-G [Tamura et al., 1991], ETERNA [Wenzel, 1996], the numerical procedure of Amoruso et al. [2000], VAV [Venedikov et al., 2003] and *clearstrain+* [Langbein, 2010]. Each software adopts a model of the strain signal and can consider different strain components. Among others, barometric pressure and Earth tides are the strain sources whose effects have been widely studied. They are modelled similarly in all the softwares and they can be easily estimated automatically. The effects of the tidal variations are typically considered as the sum of variable harmonics of different amplitude and phase, with observed tidal factors and phase lags to be estimated from the theoretical values [e. g. Cartwright and Tyler, 1971; Cartwright and Edden 1973; Tamura, 1987]. The barometric pressure contribution is usually estimated with a regression model applied on the recorded barometric pressure signal. The effects of other strain sources such as precipitations could be modelled [Matsumoto et al., 2003; Hsu et al., 2015] but require at least records of rainfall in real-time. Moreover, transient variations associated to tectonic and volcano processes are not known *a priori* and, thus, they cannot be modelled accurately except off-line with the help of an external operator. For example, the procedure of Amoruso et al. [2000] introduced the possibility of including ramps as a further strain component but they can be considered in the model only if the operator indicates the time intervals during which the ramps developed. As well, *clearstrain+* used logarithmic and exponential functions to model transient variations due to tectonic and post-seismic deformations, respectively, but they can be modelled only if the time intervals when these deformation processes occur are known. In near real-time, the presence of strain components that cannot be detected and precisely modelled and of measurement errors could cause an inaccurate estimation of the strain signal components. In order to provide a robust filtered strain signal in near real-time, we preferred to remove only the well-known contributions, namely the Earth tide and the pressure changes, and focus on the efficient estimation of the related filter parameters. To avoid spurious effects, the parameter estimation and the evaluation of the filtering performances were conducted in periods when other strain components, than the pressure and the tidal components, were negligible. Therefore, we looked for periods when precipitation did not occur and the Etna activity was very low. Moreover, we checked and removed steps, outliers, gaps and corrupted data in order to obtain an estimation of the filter parameters as reliable as possible. We analyzed a very large time window spanning from November 2011, when the DRUV strainmeter was installed, to April 2021. The multiparametric weather network managed by SIAS (Servizio Informativo Agrometeorologico Siciliano, www.sias.regione.sicilia.it) provided the precipitation data for the analysis. In particular, we referred to the measurements recorded by the Bronte station, which is the nearest station to the DRUV strainmeter, located on the same volcano flank at approximately 8 km away. The volcano activity was checked by referring to the recent work of Andronico et al. [2021], which provided a useful list of all the paroxysmal episodes occurred from 1986 to 2021 at the Etna volcano. Only two long-term windows were found to be appropriate: 06 July 2016 – 06 August 2016 and 01 May 2020 – 30 May 2020. We decided to use the signal recorded in 2020 as *training signal* for the parameter estimation while the signal recorded in 2016 was used as *testing signal* for analyzing the filtering performance. The software BAYTAP-G was used for the parameter estimation and was adapted for the filtering operations in near real-time. It is important to underlie that the recorded strain signals are usually affected also by a long-term drift which is mainly due to both the relaxation of the drilled hole and the curing of the cement [i.e. Roeloff and Linde, 2007; Bonaccorso et al., 2016; Canitano et al., 2021]. The drift can persist from months to years after the installation and it decreases exponentially with time. Before proceeding with the parameter estimation, the long-term drift component was removed.

3. Parameter estimation

The mathematical model of the filter implemented in BAYTAP-G considers the recorded strain signal as the sum of a tidal, a pressure and a filtered component. The tidal component is modelled by summing theoretical harmonic functions, α_m and β_m, considered in M groups with constant amplitude and phase and scaled to the measured tidal signal through the tidal factors A_m and B_m [Tamura et al., 1991]. The pressure component can be estimated by applying a FIR filter of order q and weights b_k to the recorded barometric pressure signal p. The filtered signal is modelled as a random walk process w to which white noise is added. A_m, B_m and b_k are the filter parameters. In order to estimate them, BAYTAP-G solves a sort of "penalized" least square method in which the data are fitted using a constraint on the parameters. The estimation of the parameter is carried out by minimizing the following cost function

$$J = \sum_{i=1}^{N} \left\{ \left[y_i - \sum_{k=0}^{q} b_k p_{i-k} - \sum_{m=1}^{M} \left(A_m \alpha_{m,i} + B_m \beta_{m,i} \right) - w_i \right]^2 + D^2 (w_i - 2w_{i-1} + w_{i-2})^2 \right\} \quad (1).$$

In (1), D is a hyperparameter that influences the parameter estimation by controlling the smoothness of the signal w: the higher the value of D, the smoother w. Once D is fixed, the filter parameters can be estimated by minimizing J. BAYTAP-G tries different filtering solutions by varying the value of D in the range [D_{min} D_{max}], where D_{min} is an input parameter and D_{max} is equal to 1000. The goodness of fit of the generic filtering solution is evaluated through the Akaike Bayesian Information Criterion, ABIC [Akaike, 1980]. The minimum the ABIC, the more efficient the filtering solution. The iterative procedure implemented in BAYTAP-G to estimate the parameters is structured as follows: an initial value of D, D_1, is set to $4D_{min}$, and the ABIC corresponding to D_1, $ABIC_1$, is evaluated. At the next iteration, the value of D is increased and the second value of the ABIC, $ABIC_2$, is estimated. If $ABIC_1 < ABIC_2$ then the analyzed portion of the ABIC(D) curve has positive gradient so the minimum value of the ABIC, $ABIC_{min}$, must be found for $D < D_1$. D is then multiplied by $1/\sqrt{2}$ until $ABIC_{min}$ is found. Vice versa, if $ABIC_1 > ABIC_2$ then the gradient of the ABIC(D) curve is negative and $ABIC_{min}$ is catched for $D>D_1$ employing the multiplier $\sqrt{2}$ for the successive values of D. The iterative procedure strongly depends on the value of the input parameter D_{min} and on the analysis step of D implemented in the code. Tamura et al. [1991] underlined that this step ($1/\sqrt{2}$ or $\sqrt{2}$) is sufficient for practical purposes. We decided to investigate a wider range of D values. We increased the number of the analyzed values of D indirectly, namely by trying different values of D_{min}. Preliminary analysis showed that the optimal value of D_{min}, the one that provides D values that minimizes the ABIC, is located in the range [0 1]. Therefore, we decided to investigate values of D_{min} in the range [0 1] with a step of 0.01. The range [1 100] was analyzed as well but with a sparser step of 1. The number of analyzed filtering solutions was further increased by employing different values of the order of the FIR filter applied to the atmospheric pressure signal, q. We exploited the whole range of values of q admissible by BAYTAP-G, namely [0 72], with an analysis step of 1. The values of q were used in combination with the inspected values of D_{min} for a total of 14600 investigated couples (q, D_{min}). The goodness-of-fit of each filtering solution was evaluated employing the same ABIC criterion.

An important aspect that needs to be investigated for near real-time applications is the sampling time of the recordings. BAYTAP-G was designed and tested to analyze signals sampled at time interval of 1 hour [Tamura, 2000]. It is obvious that for surveillance applications this sampling interval is too high. Therefore, lower sampling times have been investigated to prove the efficiency of BAYTAP-G for near real-time processing at lower sampling time. In particular, we investigated three sampling times, t_c: 1 hour, 10 minutes and 5 minutes. An example of efficient filtering solution is presented in Figure 2.

The *training signal* recorded with a sampling time of 5 minutes (Figure 2a) is shown together with the related tidal (Figure 2b), pressure (Figure 2c) and filtered strain components (Figure 2d) obtained using the couple (q, D_{min}) = (10, 0.91). This solution was found by comparing the ABIC values of all the inspected couples (q, D_{min}). In Figure 3, the ABIC values are plotted against the parameter q for all the couples (q, D_{min}) employed for filtering the *training signal*.

In particular, the results for the signal recorded with a sampling time of 1 hour (Figure 3a), 10 minutes (Figure 3b) and 5 minutes (Figure 3c) are presented. The red dots represent the *q-optimal* couples (q, $D_{min,opt}$), namely all the combinations (q, D_{min}) that provided the lowest value of the ABIC for each analyzed q. In order to choose the most efficient (q, $D_{min,opt}$) combination among all the *q-optimal* couples, our approach was not to select the (q, $D_{min,opt}$)

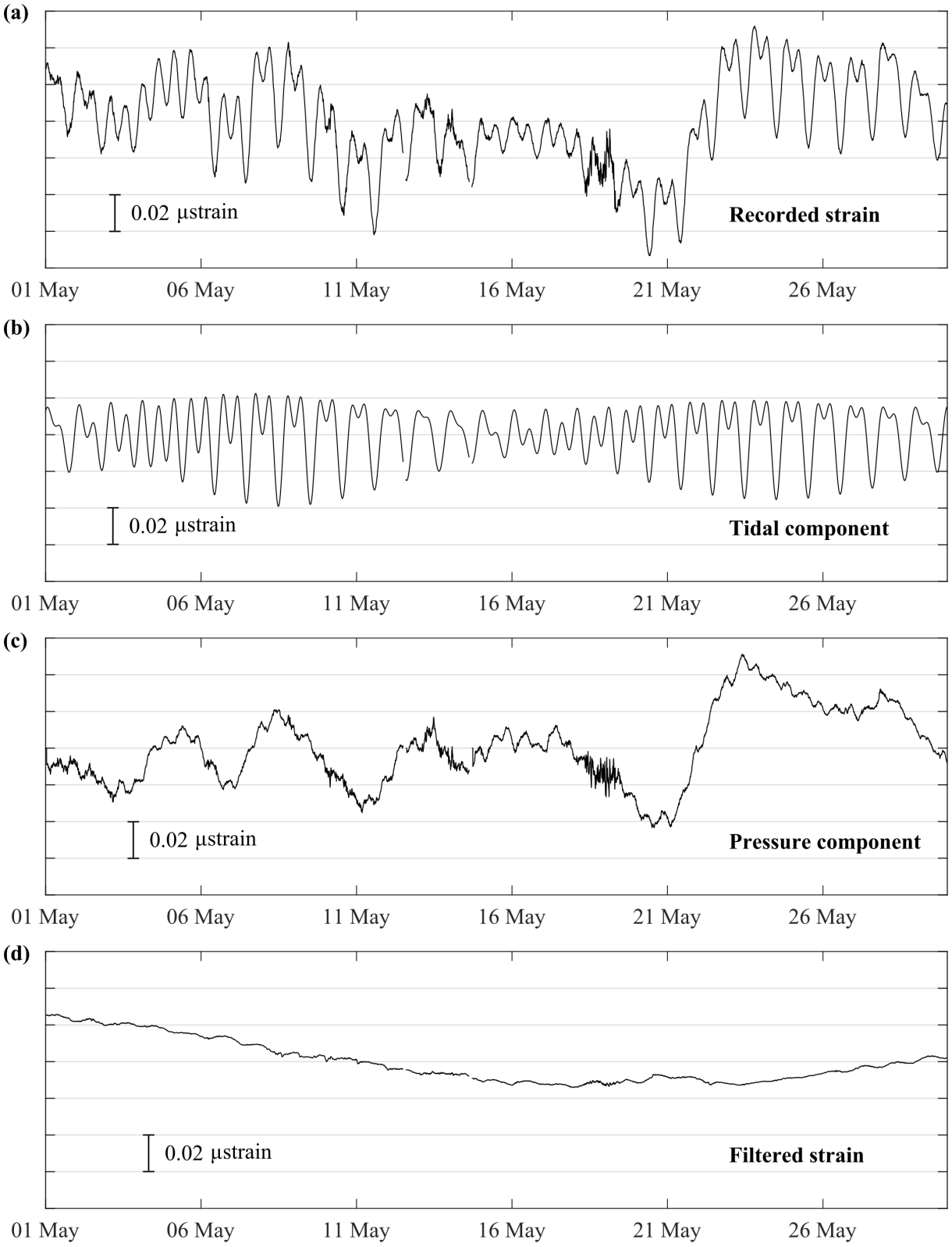

Figure 2. *Training signal* recorded from 01 May 2020 to 30 May 2020 with a sampling time of 5 minutes (a) plotted together with the tidal (b), pressure (c) and filtered (d) components obtained using the parameter couple $(q, D_{min}) = (10, 0.91)$.

combination which lead to the absolute minimum value of the ABIC. Instead, we chose the $(q, D_{min,opt})$ couple that represents a compromise between the value of the ABIC and the number of parameters involved in the model: (1, 0.03) for $t_c = 1$h, (5, 0.95) for $t_c = 10$ min and (10, 0.91) for $t_c = 5$ min. The estimated values of the tidal factors A_m

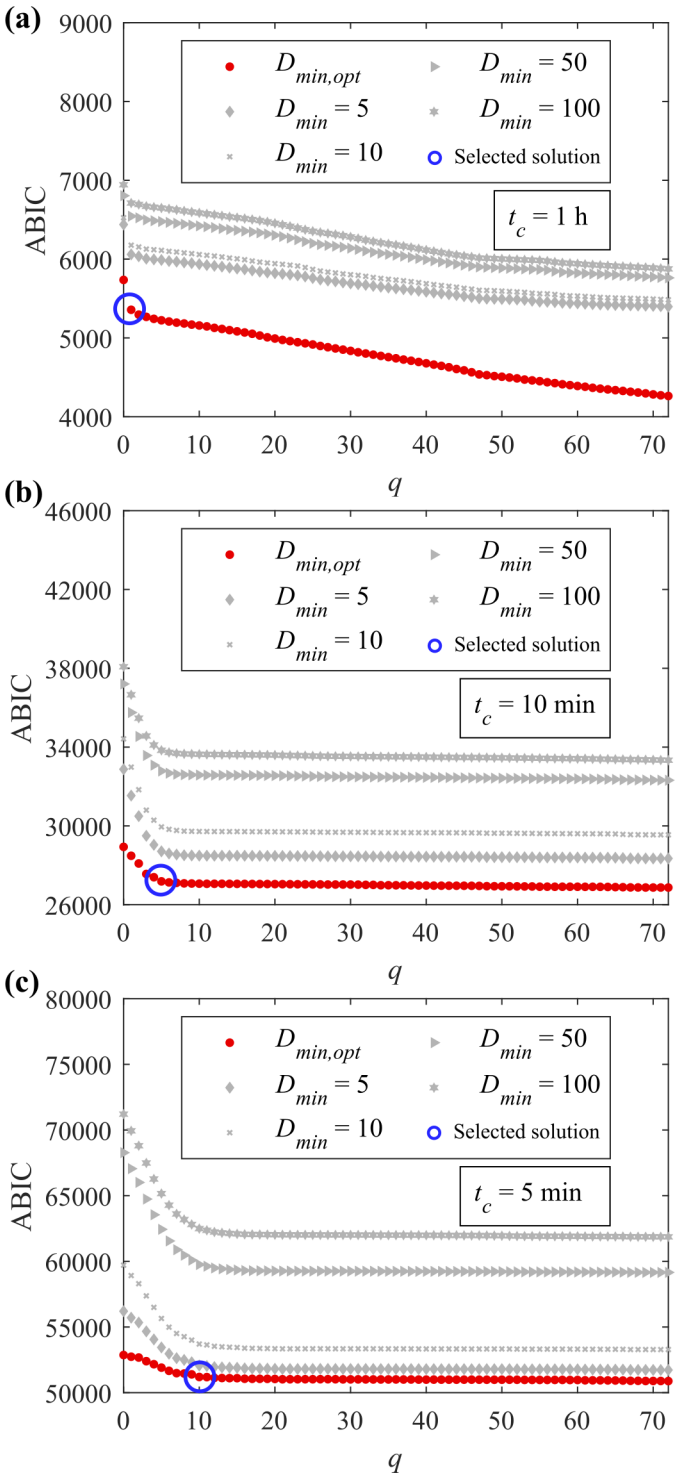

Figure 3. Values of the ABIC related to all the investigated couples (q, D_{min}) employed for filtering the *training signal* recorded at sampling time of 1 hour (a), 10 minutes (b) and 5 minutes (c). Red dots represent the couples that provided the lowest value of the ABIC for each analyzed q. The blue circles represent the selected efficient filtering solutions.

and B_m and the atmospheric pressure coefficients b_k are reported for all the analyzed sampling time in Appendix A in Table A1 and Table A2, respectively. The same procedure was implemented for the estimation of the filter parameters related to the *testing signal*. The (q, $D_{min,opt}$) couples are (1, 0.37) for t_c = 1h, (6, 0.37) for t_c = 10 min and (14, 0.64) for t_c = 5 min. The related tidal factors and atmospheric pressure coefficients are presented in Appendix B in Table B1 and Table B2, respectively.

4. Evaluation of the filtering performance

The performances of the estimated filtering solutions were evaluated analyzing the root mean square (RMS) of the signals. The first step was to compare the RMS of the recorded signals with the corresponding filtered signals. Different time scales, d, from 3 hours (typical duration of a lava fountain at Etna volcano) to 30 days (maximum length of the time window under study) were analyzed. For $d < 30$ days, the RMS was evaluated as the average value of the RMS calculated in moving windows of length d over the analyzed time period. For each time windows, we considered the signal minus its average value evaluated on d, to partially remove the drift term due to deformation processes acting on time scale higher than d. In Table 1, the RMS of the recorded *training signal*, $RMS_{r,tra}$, is presented with the RMS of the respective filtered signal, $RMS_{f,tra}$ for the different analyzed time scale d. Both the $RMS_{r,tra}$ and the $RMS_{f,tra}$ values, at a fixed time scale d, do not significantly vary with the sampling time which means that the sampling time does not cause any significant increase or decrease in both recorded and filtered signal sensitivity to strain variations.

Time scale, d	t_c = 1 h		t_c = 10 min		t_c = 5 min	
	$RMS_{f,tra}$	$RMS_{r,tra}$	$RMS_{f,tra}$	$RMS_{r,tra}$	$RMS_{f,tra}$	$RMS_{r,tra}$
3 hours	0.19	4.80	0.22	4.10	0.22	4.02
1 day	0.80	13.83	0.97	13.81	0.91	13.81
14 days	6.44	23.33	6.45	23.26	6.24	23.26
30 days	11.04	24.08	11.76	24.08	11.39	24.08

Table 1. Values of the RMS in nanostrain (10^{-9}) of the recorded, $RMS_{r,tra}$, and filtered, $RMS_{f,tra}$, *training signal* evaluated on different time scales d, for different sampling times t_c.

The RMS of the recorded *training signal* is of order of few nanostrain only for $d = 3$ hours ($\approx 4*10^{-9}$) while it is of order of 10^{-8} for the rest of the analyzed time scales. The filtering process always brought benefits since $RMS_{f,tra} < RMS_{r,tra}$ for each analyzed d and for each t_c. In particular, the RMS decreased of one or two order of magnitude in case of time scales less than one day, reaching values of $\approx 10^{-10}$, while it decreased of one order of magnitude for time scales of few days, namely $\approx 10^{-9}$. In case of larger time scales of about one month, the RMS of the filtered signals decreased by a factor of ≈ 2 with respect of the recorded signal. Same considerations can be done by analyzing the RMSs of both the recorded, $RMS_{r,tra}$, and the filtered, $RMS_{r,tra}$, *testing signal* reported in Table 2.

By comparing the RMS values of the filtered solutions of both the *training* and the *testing* signals it is shown that all the RMS values of the filtered *testing signal*, at fixed time scale, are lower than the respective values of the *training signal* for the different sampling times. This means that the filtering process carried out on the *testing signal* was more efficient than the one performed on the *training signal*. However, it is worth noting that the differences are, in any case, of order, or even less, than the RMS itself. Therefore, beyond all possible explanations in these discrepancies, one of the two estimated sets of parameters can be equally chosen since they can be considered equivalent in terms of filtering efficiency, at least at the analyzed time scales and in the analyzed time periods.

We decided to employ the parameters estimated from the signal recorded in the most recent time window, namely the *training signal*, and test them for filtering strain signals recorded in different idoneous time periods. The *testing signal* was used to this scope. The filtering solution of the *testing signal* obtained with the *training signal* parameters was compared with the one obtained with the parameters estimated on the *testing signal* itself. We present the case of signal sampled every 5 minutes which is of major interest for near real-time applications. In Figure 4, the *testing signal* is plotted together with the two analyzed filtered solutions of the recorded signal. There is a good agreement

of the filtered signals that means that both the filtering solutions are quite efficient. The RMS values of the signal filtered with the parameters estimated from the *training signal* is 0.26, 1.11, 2.62 and 3.37 nanostrain for time scale of 3 hours, 1 day, 14 days and 1 month. If one compares these values with the ones of Table 2, which represent the efficient filtering solution of the *testing signal*, it can be easily verified that the RMS values are of the same order of magnitude and thus the small differences between the two analyzed filtered solutions can be neglected.

Time scale, d	t_c = 1 h		t_c = 10 min		t_c = 5 min	
	$RMS_{f,test}$	$RMS_{r,test}$	$RMS_{f,test}$	$RMS_{r,test}$	$RMS_{f,test}$	$RMS_{r,test}$
3 hours	0.12	4.79	0.14	4.03	0.17	3.94
1 day	0.41	12.86	0.46	12.93	0.59	12.93
14 days	2.29	15.64	2.34	15.72	2.45	15.72
30 days	3.01	15.64	3.13	15.72	3.05	15.72

Table 2. Values of the RMS in nanostrain (10^{-9}) of the recorded, $RMS_{r,test}$, and filtered, $RMS_{f,test}$, *testing signal* evaluated on different time scales d, for different sampling times t_c.

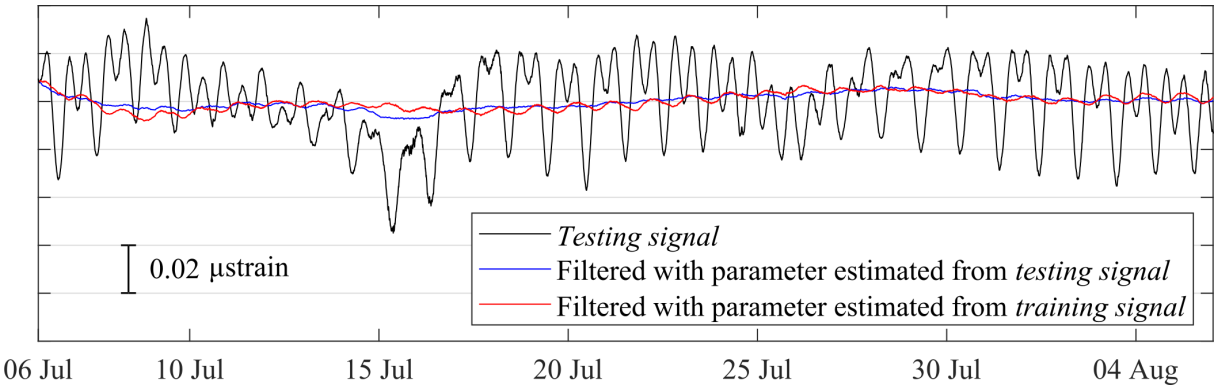

Figure 4. *Testing signal* recorded from 06 July 2016 to 06 August 2016 with a sampling time of 5 minutes, in black, plotted together with two possible filtering solutions: one obtained with parameters estimated on the *testing signal* (blue) and one obtained with filtering parameters estimated from the *training signal* (red).

5. STRALERT at INGV-OE Surveillance Room

To provide both the recorded and the filtered DRUV signals to the INGV-OE Surveillance Room the software STRALERT was developed. It was written in MATLAB environment (R2020b) to routinely perform the operations of signal reading, filtering and transferring. The flow chart of STRALERT is presented in Figure 5.

The software can be launched with the script *STRALERT.m* which contains all the code lines where the input parameters can be set. At the first run, the function *initialization.m* is launched. It executes preliminary operations to check the compatibility of the input parameters with the input signals, namely the recorded strain signal and the recorded barometric pressure signal. Successively, the software executes the script *maincode.m* which groups all the instructions that will be performed routinely for reading, filtering and transferring the signals. STRALERT encloses an updated version of the software BAYTAP-G. Indeed, since the current version of BAYTAP-G did not

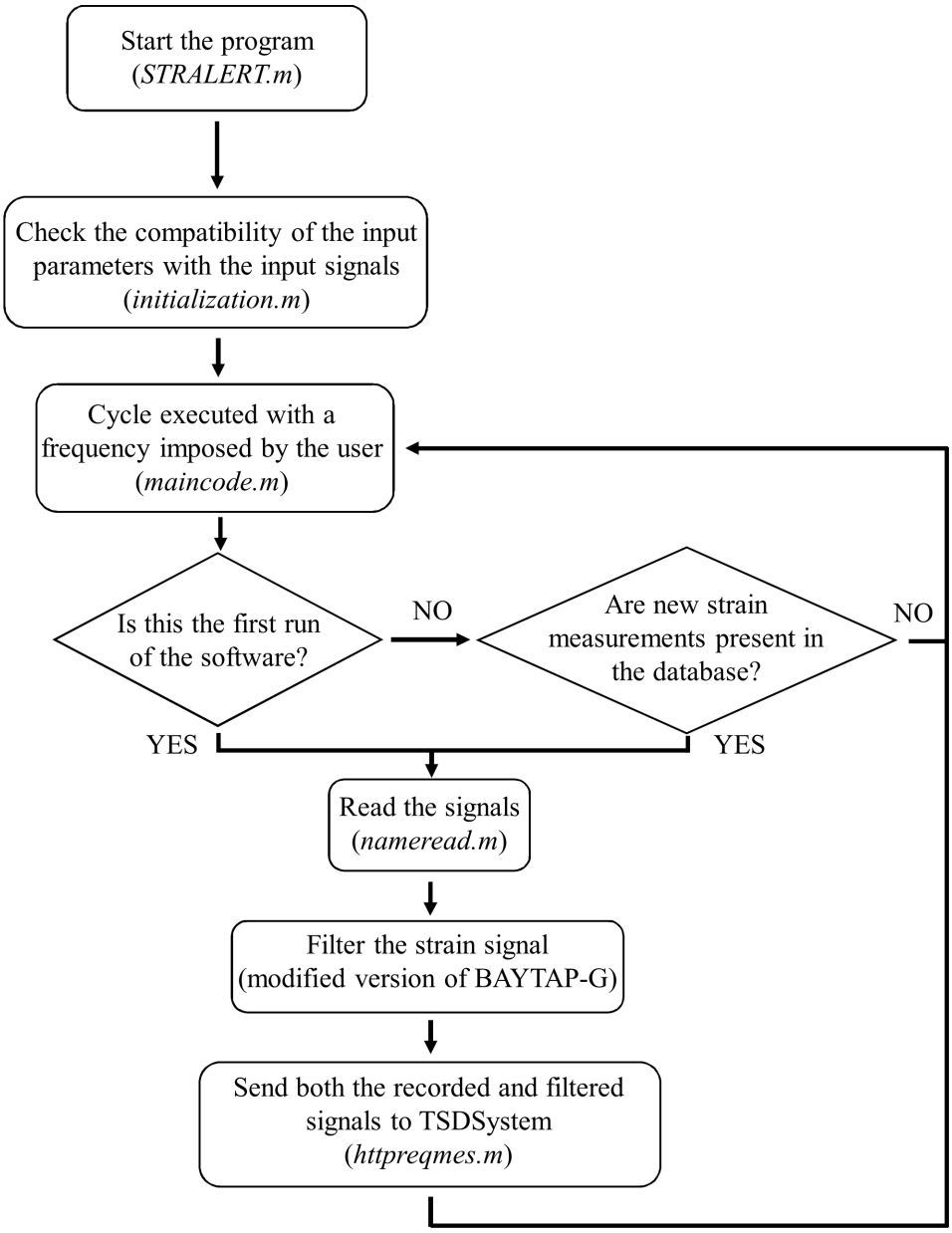

Figure 5. Flow chart of STRALERT.

allow using a given set of filter parameters as inputs, the original code of BAYTAP-G was modified. We introduced a new processing module that allows bypassing the parameter estimation procedure implemented in the software and, instead, uses a set of filter parameters previously computed and stored in a *.txt* file. The parameter reported in Table A1 are used for the signal filtering. In addition, the improved version of BAYTAP-G was further optimized for near real-time applications by avoiding the writing of some output files useful only for analysis purposes. These modifications increased the processing time of the software of about 60%. The filtered and the recorded signals are transferred through HTTP request messages to TSDSystem, the database in use in the INGV-OE Surveillance Room to store and visualize time series [Cassisi et al., 2015].

Examples of the output of STRALERT are shown to present the results obtained by this useful tool. In the following figures, some examples of strain changes occurred concurrently with some eruptive events are reported. In Figure 6, the recorded (Figure 6a) and the filtered (Figure 6b) DRUV signals are shown for the time period 12 June 2021 – 11 July 2021 as displayed in the Surveillance Room. In this time window, an intense eruptive activity of the Etna volcano took place. Each step-like change in the strain signal is related to the decompression of the volcano edifice due to lava fountain events.

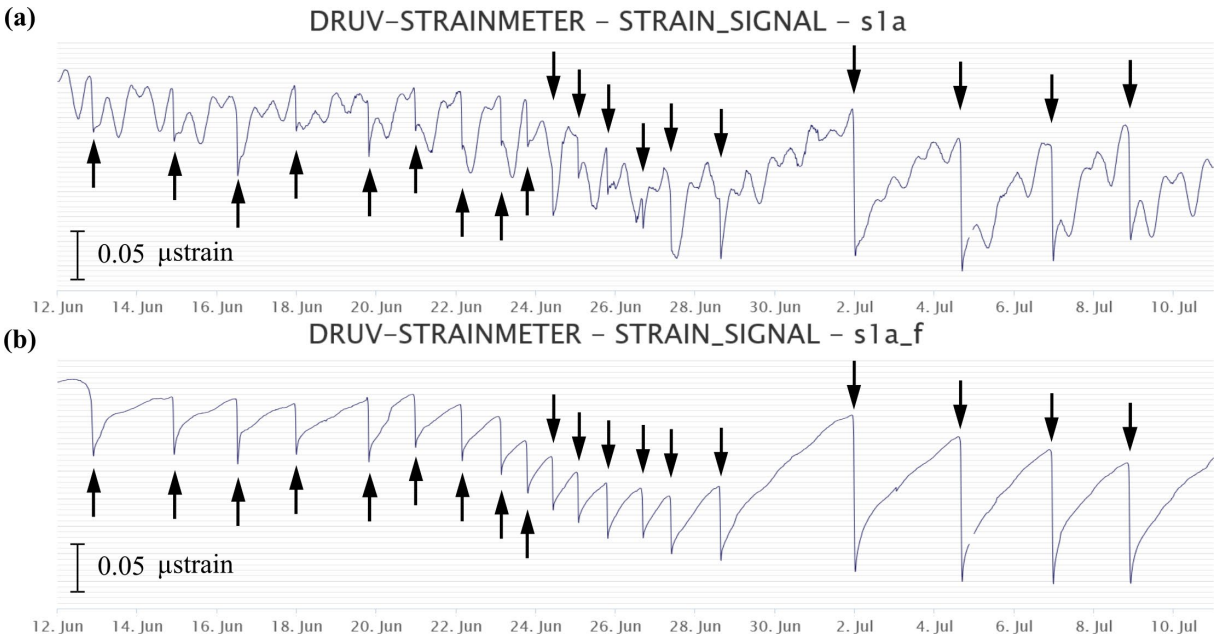

Figure 6. Example of the recorded (a) and the filtered (b) strain signals as shown in TSDSystem from 12 Jun 2021 to 11 July 2021. Negative strain changes correspond to dilatation of the rock surrounding the sensor. Black arrows indicate lava fountains. The scales and the arrows are added for a better comprehension.

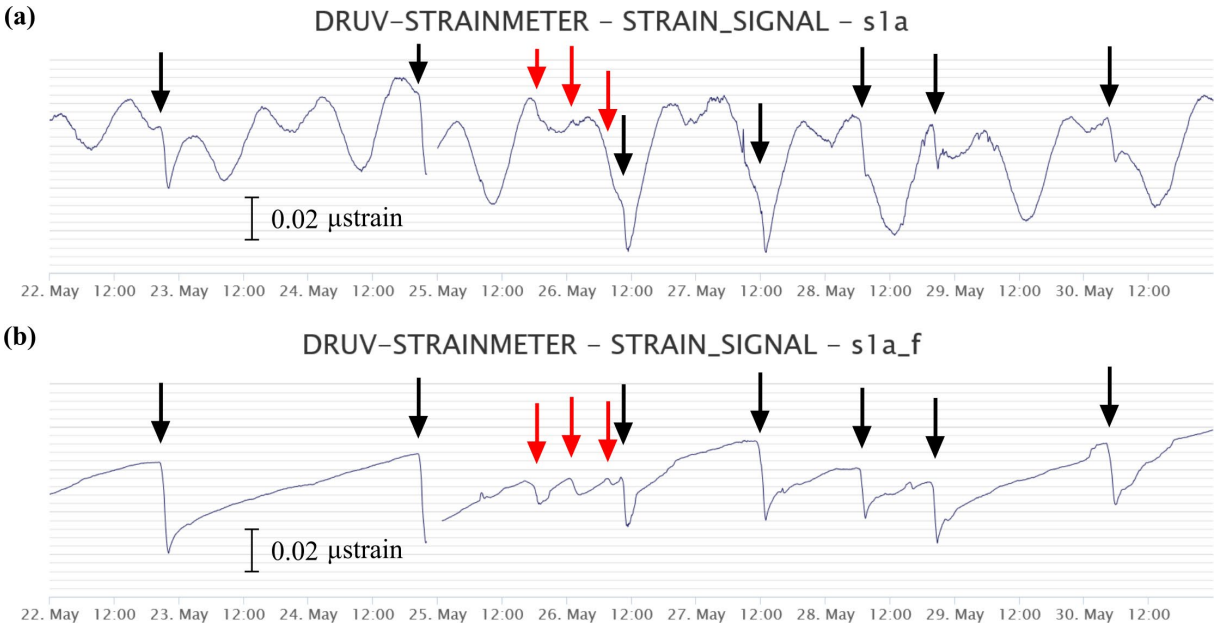

Figure 7. Recorded (a) and the filtered (b) strain signals shown on TSDSystem in the period 22 May 2021 – 31 May 2021. Black arrows indicate lava fountain events while the red arrows strombolian activity episodes. The ultra-small negative strain changes ($\approx 10^{-9}$) concurrently with the strombolian episodes are visible only on the filtered signal.

The beginning and the ending of the changes mark the onset and the conclusion of the eruptive event [Bonaccorso et al., 2016]. The events occurred in July are clearly visible in both the recorded and filtered signal exhibiting negative strain changes of the order of 10^{-7}. Instead, the lava fountains occurred in June are masked by the tidal and pressure components and are clearly detected only when the filtering is performed disclosing smaller strain changes of the order of 10^{-8}. In Figure 7, the recorded (Figure 7a) and the filtered (Figure 7b) strain signals are

presented for the time window spanning 22 May 2021 – 30 May 2021. In this period, some small lava fountains occurred together with weak strombolian activity episodes. In the recorded signal, the strain changes are hidden by the tidal and pressure variations and cannot be clearly identify. After filtering, distinct abrupt changes are shown up concurrently with the eruptive episodes and the beginning and the ending of each strain variations can be easily distinguished. Moreover, the signal enlightens ultra-small strain changes of the order of 10^{-9} observed concurrently with the three strombolian episodes occurred from 25 May 2021 to 26 May 2021 which are unrecognizable in the recorded raw strain signal.

6. Conclusions

Volcano monitoring and surveillance could greatly benefit of the availability of near-real time strain signals, since they provide a direct measurement of volcano deformation with a resolution unachievable with other geodetic techniques. However, the recorded strain signal is affected by disturbances that mask ultra-small strain changes due to volcanic processes. In order to provide an appropriately filtered strain signal in near-real time to Surveillance Room at INGV-OE, we implemented the software STRALERT, which automatically processes the recorded strain and reduces the disturbing components.

By employing and adapting the BAYTAP-G code, STRALERT filters the incoming signal from the continuously running DRUV station using a set of filter parameters previously defined and assessed. This allows for a robust filtering process avoiding unstable results. The estimation of the filter parameters carried out on appropriate periods allowed to obtain a filtered signal sensitive to ultra-small strain transients due to volcanic activity. At time scales less than one day, which are of major interest for near real-time applications, the RMS of the strain signal is improved, reaching values of $\approx 10^{-10}$ while, at time scale of few days, it can reach values of the order of 10^{-9}. This performance enables STRALERT to unravel tiny strain changes due to weak eruptive events that are completely hidden by the tidal and the pressure variations in the recorded raw signal. These small strain transients would have been undetected if filtering was not performed. Moreover, the filtered signal better shows the onset and the end of the transient strain variations allowing to easily mark the timing of the associated eruptive events. These findings show the important contribution of STRALERT to the volcano surveillance operations and the benefit for future application in volcano warning systems.

Acknowledgments. The Etna borehole strainmeter network originally benefited by the financial support of the Italian FIRB project "*Development of new technologies for the protection and defense of the territory from natural hazards*" (acronym FUMO) and PON project "*Development of research centers for the study of volcanic areas at high risk and their geothermal potential in the context of Mediterranean geological and environmental dynamic*" (acronym VULCAMED).
We sincerely thank the colleagues of the Carnegie Institution of Washington A. Linde and S. Sacks, who actively supported and coordinated the dilatometer installations on Etna and contributed to the first fundamental studies. We thank the colleagues of the Carnegie Institution of Washington M. Acierno and B. Schleigh who worked in the implementation of the instrumentation and provided useful and precious assistance.
This research benefited from fundings provided by the 2019-2021 Agreement between INGV and Italian Presidenza del Consiglio dei Ministri – Dipartimento della Protezione Civile (DPC), All. B2- WP2 -Task 9 "Ottimizzazione dell'acquisizione dei segnali ad alta precisione degli strainmeter installati in pozzo sull'Etna" (*Optimization of the acquisition of high-precision signals from the bore-hole strainmeters installed at Etna volcano*). This research also benefited from the EC H2020-FET OPEN project "*SiC optical nano-strain-meters for pico-detection in Geosciences*" (acronym SiC nano for picoGeo) grant agreement n. 863220.

References

Agnew, D. C. (1986). Strainmeters and tiltmeters, Rev. Geophys., 24, 3, 579-624.
Akaike, H. (1980). Seasonal adjustment by a bayesian modeling, J. Time Ser. Anal., 1, 1, 1-13.
Amoruso, A., L. Crescentini and R. Scarpa. (2000). Removing tidal and atmospheric effects from Earth deformation measurements, Geophys. J. Int., 140, 3, 493-499.

Amoruso, A., L. Crescentini, R. Scarpa, R. Bilham, A. T. Linde and S. I. Sacks (2015). Abrupt magma chamber contraction and microseismicity at Campi Flegrei, Italy: Cause and effect determined from strainmeters and tiltmeters, J. Geophys. Res. Sol. Earth, 120, 8, 5467-5478.

Andronico, D. A., A. Cannata, G. Di Grazia and F. Ferrari (2021). The 1986-2021 paroxysmal episodes at the summit craters of Mt. Etna: Insights into volcano dynamics and hazard, Earth Sci. Rev., 220, 103686.

Bonaccorso, A., L. Carleo, G. Currenti and A. Sicali (2021). Magma Migration at Shallower Levels and Lava Fountains Sequence as Revealed by Borehole Dilatometers on Etna Volcano, Front. Earth Sci., 9, 740505.

Bonaccorso, A., G. Currenti, A. T. Linde, and S. Sacks (2013). New data from borehole strainmeters to infer lava fountain sources (Etna 2011-2012), Geophys. Res. Lett., 40, 14, 3579-3584.

Bonaccorso, A., S. Calvari, A. T. Linde, S. I. Sacks and E. Boschi (2012). Dynamics of the shallow plumbing system investigated from borehole strainmeters and cameras during the 15 March, 2007 Vulcanian paroxysm at Stromboli volcano, Earth Planet. Sci. Lett., 357-358, 249-256.

Bonaccorso, A., A. T. Linde, G. Currenti, S. Sacks and A. Sicali (2016). The borehole dilatometer network of Mount Etna: A powerful tool to detect and infer volcano dynamics, J. Geophys. Res. Sol. Earth, 121, 6, 4655-4669.

Canitano, A., M. Mouyen, Y.-J. Hsu, A. T. Linde, S. I. Sacks and H.-M. Lee (2021). Fifteen Years of Continuous High-Resolution Borehole Strainmeter Measurements in Eastern Taiwan: An Overview and Perspectives, GeoHazards, 2, 3, 172-195.

Cartwright, D. E. and A. C. Edden (1973). Corrected Tables of Tidal Harmonics, Geophys. J. R. Astron. Soc., 33, 3, 253-264.

Cartwright, D. E. and R. J. Tayler (1971). New Computations of the Tide-generating Potential, Geophys. J. R. Astron. Soc., 23, 1, 45-73.

Cassisi, C., P. Montalto, M. Aliotta, A. Cannata and M. Prestifilippo (2015). TSDSystem: un database multidisciplinare per la gestione di serie temporali.

Currenti, G. and A. Bonaccorso (2019). Cyclic magma recharge pulses detected by high-precision strainmeter data: the case of 2017 inter-eruptive activity at Etna volcano, Sci. Rep., 9, 1, 1-7.

Currenti, G., L. Zuccarello, A. Bonaccorso and A. Sicali (2017). Borehole Volumetric Strainmeter Calibration From a Nearby Seismic Broadband Array at Etna Volcano, J. Geophys. Res. Sol. Earth, 112, 10, 7729-7738.

Dzurisin, D. (2007). Volcano deformation: geodetic monitoring techniques, Springer, Berlin, 441.

Furuya, I. and A. Fukudome (1986). Characteristics of borehole volume strainmeter and its application to seismology, J. Phys. Earth, 34, 3, 257-296.

Hsu, Y.-J., Y.-S. Chang, C.-C. Liu, H.-M. Lee, A. T. Linde, S. I. Sacks, G. Kitagawa, and Y.-G. Chen (2015). Revisiting borehole strain, typhoons, and slow earthquakes using quantitative estimates of precipitation-induced strain changes, J. Geophys. Res. Sol. Earth, 120, 6, 4556-4571.

Langbein, J. (2010). Computer algorithm for analyzing and processing borehole strainmeter data, Comput. Geosci., 36, 5, 611-619.

Linde, A. T. and S. I. Sacks (1995). Continuous monitoring of volcanoes with borehole strainmeters, in Mauna Loa Revealed: Structure, Composition, Hystory, and Hazards J. M. Rhodes and J. P. Lockwood (Editors), American Geophysical Union, Washington DC, 171-185.

Linde, A. T., K. Agustsson, S. I. Sacks and S. Ragnar (1993). Mechanism of the 1991 eruption of Hekla from continuous borehole strain monitoring, Nature, 365, 737-740.

Linde, A. T., O. Kamigaichi, M. Churei, K. Kanjo and S. I. Sacks (2016). Magma chamber recharging and tectonic influence on reservoirs: The 1986 eruption of Izu-Oshima, J. Volcanol. Geotherm. Res., 311, 72-78.

Matsumoto, N., G. Kitagawa and E. A. Roeloffs (2003). Hydrological response to earthquakes in the Haibara well, central Japan – I. Groundwater level changes revealed using state space decomposition of atmospheric pressure, rainfall and tidal responses, Geophys. J. Int., 155, 3, 885-898.

Roeloffs, E. A. and A. T. Linde (2007). Borehole observations of continuous strain and fluid pressure. In Volcano deformation 305-322.

Sacks, S., S. Suyehiro, D. W. Evertson and Y. Yamagishi (1971). Sacks-Evertson Strainmeter, Its Installation in Japan and Some Preliminary Results Concerning Strain Steps, Pap. Meteorol. Geophys., 22, 3-4, 195-208.

Tamura, Y. (1987). A harmonic development of the tide-generating potential, Bulletin d'Informations Marées Terrestres 99, 6813-6857.

Tamura, Y. (2000). Study on Precise Tidal Data Processing.

Tamura, Y., T. Sato, M. Ooe and M. Ishiguro (1991). A procedure for tidal analysis with a Bayesian information criterion, Geophys. J. Int., 104, 3, 507-516.

Van Camp, M., O. de Viron, A. Watlet, B. Meurers, O. Francis and C. Caudron (2017). Geophysics From Terrestrial Time-Variable Gravity Measurements, Rev. Geophys., 55, 4, 938-992.

Venedikov, A. P., J. Arnoso and R. Vieira. (2003). VAV: A program for tidal data processing, Comput. Geosci., 29, 4, 487-502.

Voight, B., A. T. Linde, S. I. Sacks, G. S. Mattioli, R. S. J. Sparks, D. Elsworth, D. Hidayat, P. E. Malin, E. Shalev, C. Widiwijayanti, S. R. Young, V. Bass, A. Clarke, P. Dunkley, W. Johnston, N. McWhorter, J. Neuberg, and P. Williams (2006). Unprecedented pressure increase in deep magma reservoir triggered by lava-dome collapse, Geophys. Res. Lett., 33, 3, L03312.

Wenzel, H.-G. (1996). The nanogal software: earth tide processing package ETERNA 3.30, Bulletin d'Informations Marées Terrestres 124, 9425-9439.

***CORRESPONDIG AUTOR: Luigi CARLEO**,
Istituto Nazionale di Geofisica e Vulcanologia, Sezione di Catania – Osservatorio Etneo,
Catania, Italy,
email: luigi.carleo@ingv.it